

# A thermospheric model based on satellite drag data

by

F. BARLIER\*, C. BERGER\*, J.L. FALIN\*, G. KOCKARTS\*\* and G. THUILLIER\*\*\*

**ABSTRACT.** — *A three-dimensional thermospheric model is developed in terms of spherical harmonics by using satellite drag data which cover a time-period of almost two solar cycles. The model gives total density, partial densities (He, O, N<sub>2</sub>) and temperature as a function of solar and geomagnetic activity, local time, day of the year, altitude and latitude. The partial densities given by the model are in rather good agreement with various in situ measurements which were, however, not involved in the construction of the model. The amplitude of the winter helium bulge is, however, less important than the value obtained from mass spectrometer measurements.*

**RESUME.** — *Un modèle thermosphérique à trois dimensions est établi par une analyse en harmoniques sphériques d'un grand nombre de données de freinage de satellites couvrant pratiquement une période de deux cycles d'activité solaire. La densité totale, les concentrations partielles (He, O, N<sub>2</sub>) et la température sont exprimées en fonction de l'activité solaire et géomagnétique, de l'heure locale, du jour de l'année, de l'altitude et de la latitude. Les concentrations partielles données par le modèle sont en accord satisfaisant avec diverses mesures in situ qui n'ont cependant pas été incluses dans l'élaboration du modèle. Toutefois, l'amplitude du renflement hivernal de l'hélium est moins importante que la valeur déduite des mesures par spectrométrie de masse.*

## 1. Introduction

It was realized very soon after the launching of the first artificial satellites that the fluctuations of the orbital period were related to variations in the upper atmosphere (Jacchia, 1959; Groves, 1959; Priestler, 1959; King-Hele and Walker, 1959). Since that time a permanent effort has been made to obtain reliable atmospheric models. The perfect atmospheric model should be able to represent all the physical properties of the terrestrial atmosphere. At present time it is, however, impossible to build an atmospheric model without some working hypotheses and the weakness of a model usually appears when one or several initial hypotheses are proved to be unsatisfactory or when new experimental data are available.

The most widely used semi-empirical models are those of Jacchia (1965, 1971 a) which are based on satellite drag data combined with the assumption of diffusive equilibrium. Most of the variations occurring in the upper atmosphere were deduced from satellite drag data. This technique, actually, leads to a remarkable knowledge of the upper atmosphere, although total density is the best known quantity. The major thermospheric variations were discovered by this technique.

More recently mass spectrometer measurements, optical measurements, incoherent scatter sounders have provided new informations on the various atmospheric constituents and on the atmospheric temperature Hedin, Mayr, Reber, Spencer and Carignan, 1974; Alcaydé, Bauer and Fontanari, 1974; von Zahn, Köhnlein, Fricke, Laux, Trinks and Volland, 1977; Hedin, Salah, Evans, Reber, Newton, Spencer, Kayser, Alcaydé, Bauer, Cogger and McClure, 1977a; Thuillier, Falin and Wachtel, 1977a, Thuillier, Falin and Barlier 1977b; Hedin, Reber, Newton, Spencer, Brinton and Mayr, 1977b).

Although these models give valuable informations on the physical structure of our upper atmosphere it is

\* Centre d'Etudes et de Recherches Géodynamiques et Astronomiques, 8, Boulevard Emile-Zola, F-06130 Grasse (France).

\*\* Institut d'Aéronomie Spatiale de Belgique, 3, Avenue Circulaire, B-1180 Bruxelles (Belgique).

\*\*\* Service d'Aéronomie du CNRS. Boîte Postale n° 3, F-91370 Verrières-Le-Buisson (France).

seem useful to present here a new model based on satellite drag data for two major reasons. Firstly, the existence of a global exosphere temperature model (Thuillier *et al.*, 1977a, b) based on direct optical determinations of the temperature, provides an important hint to the interpretation of the drag data. Secondly the drag data used in this paper have a very good spatial and time coverage over almost two solar cycles.

The modelling procedure is described in section 2 as well as the various assumptions used in this work. Section 3 gives an overview of the geophysical characteristics coming out of the model and a listing of the FORTRAN subroutines required for practical uses of the models is given in appendix.

## 2. Modelling procedure

### 2.1. General principle

The majority of satellite drag data are obtained in the height region between 200 km and 1200 km. By numerical integration along the orbit (see Jacchia and Slowey 1962; Roemer, 1963) or with help of analytical expressions (see King-Hele, 1966; Vercheval, 1974), it is possible to compute the atmospheric total density in the vicinity of the satellite perigee. Without any further assumption or information nothing can be deduced on the composition and temperature. The total densities obtained by this technique actually represent the a priori unknown contribution of molecular nitrogen, molecular and atomic oxygen, helium and hydrogen.

As a consequence of diffusive separation above 100 km altitude, molecular nitrogen  $N_2$ , atomic oxygen  $O$  and helium  $He$  successively become the major atmospheric constituent (Kockarts and Nicolet, 1963) responsible for the satellite drag in the 200 km – 1200 km height range. It is, therefore, possible to identify practically the observed total density with the density of one of these constituents over certain height ranges which vary with geophysical conditions. Since molecular oxygen  $O_2$  and atomic hydrogen  $H$  are never major components between 200 km and 1200 km altitude, some hypotheses must be adopted for their vertical distribution because  $N_2$ ,  $O$  and  $He$  can only be deduced after subtraction of the small  $O_2$  and  $H$  contributions to the total density. Furthermore, a horizontal and vertical temperature distribution must be adopted in order to compute the distributions of the individual components. This outline of the general procedure will be detailed in the following subsections.

### 2.2. Working hypotheses

In order to compute vertical distributions of the atmospheric constituents, one has to adopt a vertical temperature distribution. Numerical integration of the

diffusive equilibrium equations is eliminated when the temperature  $T$  is given as a function of altitude  $z$  by the expression suggested by Walker (1965):

$$T(z) = T_{\infty} - (T_{\infty} - T_{120}) \exp(-\sigma \zeta) \quad (1)$$

where  $T_{\infty}$  is the thermopause temperature and  $T_{120}$  is the constant temperature at the lower boundary of 120 km altitude. The geopotential altitude  $\zeta$  is given by:

$$\zeta = \frac{(z - 120)(R + 120)}{R + z} \quad (2)$$

with  $R = 6356.77$  km. The quantity  $\sigma$  is related to the temperature gradient parameter  $s$  by:

$$\sigma = s + (R + 120)^{-1} \quad (3)$$

It has been shown (Alcaydé *et al.* 1974) from the St. Santin incoherent scatter data, that the temperature and its gradient at the lower boundary change with season. Alcaydé, Bauer, Hedin and Salah (1977) have shown that the  $s$  parameter is equal to 0.019, 0.022 and 0.025, respectively for equinox, summer and winter conditions at 45°N. The temperatures  $T_{120}$  are respectively 375 K, 390 K and 365 K. Such variations are, however, not yet known on a worldwide basis. For this reason we adopt a constant temperature  $T_{120} = 380$  K and a constant  $s = 0.02$ . The temperature gradient parameter deduced by Hedin *et al.* (1974) is  $(0.0215 \pm 0.0011)$  and their  $T_{120}$  is equal to 355 K. It should be realized that at the present time no atmospheric model can give a perfect representation of the temperature between 100 km and 200 km altitude. Theoretical models are hindered by the physical and mathematical difficulties in lowering the boundary level to an altitude such that the temperature computed at 120 km results from a real energy balance (Kockarts, 1975). The thermal properties of the lower boundary depend simultaneously on the solar ultraviolet flux, the downward kinetic and turbulent heat conduction and the transport of oxygen which is a function of the eddy diffusion coefficient and of photochemical processes. Donahue and Carignan (1975) have shown that between 100 km and 120 km larger temperature gradients than usually in standard models are required to explain the green nightglow emission observed from the OGO-6 satellite. For thermopause temperature between 800 K and 1500 K the temperature gradient obtained from equation (1) at 120 km range from 8 K/km to 23 K/km with  $s = 0.02$  and  $T_{120} = 380$  K. These values are compatible with the results of Donahue and Carignan (1975) if a constant eddy diffusion coefficient of  $5 \times 10^5 \text{ cm}^2 \text{ s}^{-1}$  is used independent of latitude.

The thermopause temperature  $T_{\infty}$  must also be known for any use of expression (1). In the present paper we adopt the model of Thuillier *et al.* (1977b) which combines the optical data obtained with a Fabry-Perot inter-

ferometer on board the OGO-6 satellite and temperatures from incoherent scatter data obtained at Millstone Hill, St. Santin and Arecibo. The worldwide temperature distribution is therefore known from equation (1) where the geophysical variations are included through the model of  $T_\infty$ .

Finally it is necessary to specify how  $O_2$  and  $H$  are taken into account in the model. Atomic hydrogen is always a minor constituent below 1 200 km. Its contribution to the total density is almost negligible over the whole height range covered by the model. For the determination of the helium density above 500 km altitude, atomic hydrogen has been however, subtracted from the total density. This has been done by using the hydrogen densities given by the model of Hedin *et al.* (1977b).

Above 200 km altitude the  $O_2$  contribution to the total density is smaller than 5 %. It is, therefore, reasonable to adopt a constant  $O_2$  density at 120 km and to compute its vertical distribution in diffusive equilibrium with the temperature profile given by equation (1). The constant  $O_2$  concentration at 120 km is  $4.75 \times 10^{10} \text{ cm}^{-3}$ . This procedure cannot lead to correct molecular oxygen distributions below 200 km since the diffusive equilibrium hypothesis is not fully correct in that height region (Zimmerman and Keneshea, 1976). Furthermore it will be shown later that the atomic oxygen concentration obtained with the present mode is not constant at 120 km altitude. In this case molecular oxygen should also change since both constituents are related through the photodissociation and recombination processes even if the transport effect is not identical for each one (see Banks and Kockarts, 1973). The  $O - O_2$  problem is actually the fundamental reason for which almost all thermospheric models have their lower boundary at 120 km altitude. Below that height a strong departure from diffusive equilibrium occurs and the coupling between continuity, momentum and energy equations is absolutely necessary to obtain consistent solutions.

### 2.3. Mathematical formulation

The various concentrations (or densities) contributing to the total density are expanded in terms of spherical harmonics in a way similar to Hedin *et al.* (1974). The respective concentrations  $n_i(z)$  for  $N_2$ ,  $O$  and  $He$  are represented by:

$$n_i(z) = A_{1i} \exp [G_i(L) - 1] \times f_i(z) \quad (4)$$

The function  $f_i(z)$  results from the integration of a diffusive equilibrium distribution with the temperature profile given by equation (1). One obtains (Walker, 1965; Bates, 1959):

$$f_i(z) = \left( \frac{1 - a}{1 - a e^{\sigma \xi}} \right)^{1 + \alpha_i + \gamma_i} \exp [-\sigma \gamma_i \xi] \quad (5)$$

$$\text{where:} \quad a = (T_\infty - T_{120})/T_\infty \quad (6)$$

and  $\alpha_i$  is the thermal diffusion factor which is taken equal to  $-0.38$  for the and zero for  $N_2$  and  $O$  (Kockarts, 1963). The dimensionless parameter  $\gamma_i$  is given by :

$$\gamma_i = (m_i g_{120})/\sigma k T_\infty \quad (7)$$

where  $m_i$  is the molecular mass of constituent  $i$ ,  $k$  is Boltzmann's constant and  $g_{120}$  is the acceleration of gravity at 120 km altitude. In equation (4),  $A_{1i}$  is a constant which is identical to the concentration of constituent  $i$  at the lower boundary only if the function  $G_i(L)$  reduces to one, as in the case of molecular oxygen. For  $N_2$ ,  $O$  and  $He$ , the values of  $A_{1i}$  are obtained through a least square technique used for the determination of the coefficients in  $G_i(L)$ . The functions  $G_i(L)$  are developments in spherical harmonics and depend on the local time  $t$ , the colatitude  $\theta$  (or the latitude  $\varphi = \pi/2 - \theta$ ) the day count  $d$  in the year, the daily 10.7 cm solar flux  $F$  measured at the day  $d - 1$ , the average flux  $\bar{F}$  over 3 solar rotations centered on the day  $d$  and the three-hourly planetary index  $K_p$  taken 3 hours before  $t$ . The radioelectric flux  $F$  is not reduced to the distance of one astronomical unit. Omitting the subscript  $i$ , the function  $G(L)$  is given in a way similar to Hedin *et al.* (1974) by:

$$\begin{aligned} G(L) &= 1 + F1 + M + \sum_{q=1}^{\infty} a_q^0 P_q^0(\theta) \\ &= \beta \sum_{p=1}^{\infty} b_p^0 P_p^0(\theta) \cos [p \Omega (d - \delta_p)] \\ &+ \beta \sum_{n=1}^{\infty} \sum_{m=1}^n \left\{ c_n^m P_n^m(\theta) \cos (m \omega t) + \right. \\ &\quad \left. + d_n^m P_n^m(\theta) \sin (m \omega t) \right\} \quad (8) \end{aligned}$$

with  $\Omega = 2\pi/365$  (day $^{-1}$ ) and  $\omega = 2\pi/24$  (hour $^{-1}$ ). The  $P_n^m$  represent the associated Legendre functions which will be given explicitly later. The other symbols will be progressively defined. The development (8) will be limited in a way that 35 unknown coefficients  $A_j$  ( $j = 2$  to 36) must be determined. With the coefficient  $A_1$  of equation (4) we have 36 unknowns coefficients  $A_j$  ( $j = 1, 36$ ) for each constituent. The thermopause temperature is given by:

$$T_\infty = A_1 G(L) \quad (9)$$

where the 36 coefficients  $A_j$  are given by Thuillier *et al.* (1977b). The various terms of equation (8) are now written explicitly and the symbols  $a_q^0$ ,  $b_p^0$ ,  $\delta_p$ ,  $c_n^m$  and  $d_n^m$  are replaced by the unknown coefficients  $A_2$  to  $A_{36}$ ,  $A_1$  being always the first factor on the right hand side of equations (4) or (9).

The serie with indices  $q$  is approximated by:

$$\sum_{q=1}^{\infty} a_q^0 P_q^0(\theta) \approx A_2 P_2^0 + A_3 P_4^0 \quad (10)$$

with: 
$$P_2^0 = \frac{1}{2} (3 \sin^2 \varphi - 1) \quad (11)$$

and: 
$$P_4^0 = \frac{1}{8} (35 \sin^4 \varphi - 30 \sin^2 \varphi + 3) \quad (12)$$

The terms  $F1$  and  $M$  are defined as following:

$$F_1 = A_4 (F - \bar{F}) + A_5 (F - \bar{F})^2 + A_6 (\bar{F} - 150) \quad (13)$$

where the solar decimetric fluxes are measured in units of  $10^{-22} \text{ W m}^{-2} \text{ Hz}^{-1}$ :

$$M = (A_7 + A_8 P_2^0) K_p \quad (14)$$

The serie with indices  $p$  is approximated by:

$$\sum_{p=1}^{\infty} b_p P_p^0(\theta) \cos [p \Omega (d - \delta_p)] \approx AN1 + AN2 + SAN1 + SAN2 \quad (15)$$

The annual term ( $p = 1$ ) and the semiannual term ( $p = 2$ ) independent of the sign of the latitude are written respectively:

$$AN1 = (A_9 + A_{10} P_2^0) \cos [\Omega (d - A_{11})] \quad (16)$$

and:

$$SAN1 = (A_{12} + A_{13} P_2^0) \cos [2 \Omega (d - A_{14})] \quad (17)$$

The annual and semi annual terms which have opposite signs in both hemispheres are written:

$$AN2 = (A_{15} P_1^0 + A_{16} P_3^0 + A_{17} P_5^0) \cos [\Omega (d - A_{18})] \quad (18)$$

with:

$$P_1^0 = \sin \varphi \quad (19)$$

$$P_3^0 = \frac{1}{2} (5 \sin^2 \varphi - 3) \sin \varphi \quad (20)$$

$$P_5^0 = \frac{1}{8} (63 \sin^4 \varphi - 70 \sin^2 \varphi + 15) \sin \varphi \quad (21)$$

and: 
$$SAN2 = A_{19} P_1^0 \cos [2 \Omega (d - A_{20})] \quad (22)$$

The serie with indices  $n$  and  $m$  is approximated by:

$$\sum_{n=1}^{\infty} \sum_{m=1}^n \{ c_n^m P_n^m(\theta) \cos (m \omega t) + d_n^m P_n^m(\theta) \sin (m \omega t) \} \approx D + SD + TD \quad (23)$$

The diurnal term ( $m = 1$ ) is given by:

$$D = \{ A_{21} P_1^1 + A_{22} P_3^1 + A_{23} P_5^1 + (A_{24} P_1^1 + A_{25} P_2^1) \cos [\Omega (d - A_{18})] \} \cos \omega t + \{ A_{26} P_1^1 + A_{27} P_3^1 + A_{28} P_5^1 + (A_{29} P_1^1 + A_{30} P_2^1) \cos [\Omega (d - A_{18})] \} \sin \omega t \quad (24)$$

with:

$$P_1^1 = \cos \varphi \quad (25)$$

$$P_2^1 = \frac{3}{2} \sin^2 \varphi \quad (26)$$

$$P_3^1 = \frac{3}{2} (5 \sin^2 \varphi - 1) \cos \varphi \quad (27)$$

$$P_5^1 = \frac{1}{8} (315 \sin^4 \varphi - 210 \sin^2 \varphi + 15) \cos \varphi \quad (28)$$

The diurnal term contains a contribution which is independent of the sign of the latitude (terms  $P_1^1, P_3^1, P_5^1$ ) and a contribution variable during the year (terms  $\cos [\Omega (d - A_{18})]$ ) with a part proportional to  $P_1^1$  independent of the sign of the latitude and a part proportional to  $P_2^1$  which depends of the sign of the latitude. The semidiurnal term ( $m = 2$ ) is given by:

$$SD = \{ A_{31} P_2^2 + A_{32} P_3^2 \cos [\Omega (d - A_{18})] \} \cos 2\omega t + \{ A_{33} P_2^2 + A_{34} P_3^2 \cos [\Omega (d - A_{18})] \} \sin 2\omega t \quad (29)$$

with: 
$$P_2^2 = 3 \cos^2 \varphi \quad (30)$$

$$P_3^2 = 15 \sin \varphi \cos^2 \varphi \quad (31)$$

The semidiurnal term contains a contribution which is independent of the sign of the latitude (term  $P_2^2$ ) and a contribution variable during the year (term  $\cos [\Omega (d - A_{18})]$ ) and having the sign of the latitude (term  $P_3^2$ ). The terdiurnal term ( $m = 3$ ) is given by:

$$TD = A_{35} P_3^3 \cos 3\omega t + A_{36} P_3^3 \sin 3\omega t \quad (32)$$

with: 
$$P_3^3 = 15 \cos^3 \varphi \quad (33)$$

The coefficient  $\beta$  in equation (8) is taken equal to 1 +  $F1$  for  $O$ ,  $N_2$  and  $T_{\infty}$  whereas  $\beta = 1$  for  $He$  (see section 2.5). It is clear that the various terms of equations (8) can be combined in other ways than in expressions (10), (13), (14), (15) and (23). The truncation of the series and the grouping of the terms have been guided here by the possibility of easy comparison with other models based on similar schemes.

### 2.4. Total density data

Using the orbital elements regularly published by the Goddard Space Flight Center, a file of 12 000 total densities has been computed between 200 km and 600 km altitude over a period of 4 years. Since 80 satellites were involved in the computations, one gets a rather good geophysical distribution of the data (Barlier, Falin, I11 and Jaeck, 1973). Approximately 8 000 values have been recently added to that file (Fernandez Salgado, 1976) which contains now 20 000 densities obtained from a hundred of different satellites over a period of 6 years. Almost 50 000 total densities computed by Jacchia (1971b) and by Jacchia and Slowey (1975) have been added to the density file which constitutes the initial data base. An error in the total density can be introduced through the uncertainty of the drag coefficient and the area to mass ratio of each satellite. The drag coefficient can be estimated with an accuracy of a few percents for spherical satellites (Cook, 1966). For a non spherical satellite the drag coefficient and the area to mass ratio depend on the attitude of the satellite and the accuracy can range from a few percents up to 20 %.

The whole data base has not been used in the computational procedure described in section 2.5. Figure 1 shows the time and latitudinal distribution of the total

density data actually used in the computation of the constituent indicated above each graph. Such a distribution covers more than a solar cycle. The lower part of Fig. 1 gives also the number of total densities as a function of the mean solar decimetric flux  $\bar{F}$  and as a function of the three-hourly geomagnetic  $K_p$  index. The excellent geographical and local time coverage combined with a satisfactory distribution as a function of solar and geomagnetic activity provides a good argument for the reliability of the present model.

### 2.5. Computational technique

Molecular oxygen, atomic hydrogen and temperature are supposed to be known as described in section 2.2. The computational technique for the determination of the  $3 \times 36$  unknown coefficients in the mathematical formulation of section 2.3 is based on an iterative process.

The data for which the mass density of helium represents more than 70 % of the total density are selected by means of the reference model of Hedin *et al.* (1977a, 1977b). A first approximation of the helium density is obtained by subtracting the reference model values for  $O$  and  $N_2$  as well as the  $O_2$  and  $H$  contributions from the total density. With this first approximation, a least square fitting leads then to a first approximation for the 36 coefficients  $A_i$  required in the spherical harmonics expansion for helium. The parameter  $\beta$  is set equal to one in expression (8) and as a consequence the annual, semiannual, diurnal, semidiurnal and terdiurnal terms for helium are independent of solar activity. The helium density depends, however, on solar activity through the terms given by equations (13) and (14). With  $\beta = 1 + F1$  the difference between the helium distribution computed with (8) and the values deduced from the drag data is statistically larger than for the case  $\beta = 1$ . For atomic oxygen and molecular nitrogen, a better fit is, however, obtained with  $\beta = 1 + F1$ .

With the first spherical harmonic approximation for helium and the  $N_2$  density of the reference model, one sorts out of the data base those for which atomic oxygen represents 70 % of the total density. The approximate knowledge of the other constituents allows a determination of the atomic oxygen densities and a least square fitting leads to the first approximation for the 36 coefficients of the  $O$  spherical harmonics expansion.

With the first approximations for  $He$  and  $O$  and the distribution of  $O_2$  and  $H$ , one investigates the total densities which are characterized by 50 % molecular nitrogen. The criteria is less restrictive in order to obtain a satisfactory distribution of the data. When the  $N_2$  densities are obtained, a least square fitting leads to the first approximation for the 20 coefficients of the  $N_2$  spherical harmonics expansion. The number of coefficients is smaller since the diurnal, semidiurnal and ter-

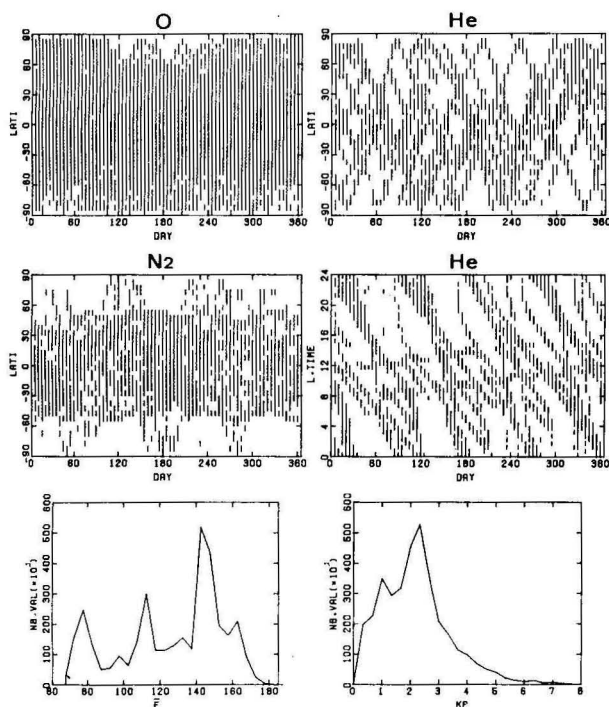


Fig. 1

Geographical and time distributions of the total density data used in the modelling of the constituent indicated above each part. The statistical distribution of the data is also given as a function of  $\bar{F}$  and  $K_p$ .

diurnal have been set equal to zero. These terms are very small and have been omitted to avoid correlations with other terms. Such fortuitous correlations could actually arise as a consequence of the smaller amount of  $N_2$  data.

A first set of coefficients is obtained in this way for  $He$ ,  $O$  and  $N_2$ . One iterates now the process until the solution becomes stable. After three iterations, a coherent solution is obtained for the major constituents  $N_2$ ,  $O$  and  $He$ . The coefficients  $A$  are given in Table 1. A check has been made that these coefficients are independent of the choice of the reference model.

### 2.6. Reliability of the solution

With the criteria adopted for the selection of the total densities  $\rho$  ( $\rho(He) \geq 0.7 \rho$ ;  $\rho(O) \geq 0.7 \rho$  or

$\rho(N_2) \geq 0.5 \rho$ ), it is clear that a large number of densities in the data base (70000 values) have not been used in the computation. The coefficients for  $He$  in Table I are obtained from approximately 8000 values of the total density. Those for  $O$  result from approximately 24000 values of the total density and 4000 values of  $\rho$  were used for the computation of the  $N_2$  coefficients.

Since the spherical harmonic analysis has been made with approximately 50 % of the amount of densities contained in our data base, it is useful to analyse how the model represents the whole set of 70000 observed densities. The ratio between each density  $\rho_{obs}$  of the data base and the computed density  $\rho_{model}$  has been averaged as a function of various geophysical parameters of the model. The results are presented on Figure 2. It

Table 1  
Coefficients  $A_j$  ( $j = 1, 36$ )

$j$	$T_\infty$	$He$	$O$	$N_2$
1	9.9980 E + 02	3.0016 E + 07	1.0320 E + 11	3.8420 E + 11
2	-3.6357 E - 03	1.6926 E - 01	-1.6598 E - 03	2.8076 E - 02
3	2.4593 E - 02	-6.2624 E - 02	-9.9095 E - 02	4.8462 E - 02
4	1.3259 E - 03	2.3799 E - 03	7.8453 E - 04	-8.1017 E - 04
5	-5.6234 E - 06	-3.1008 E - 05	-2.3733 E - 05	2.0983 E - 05
6	2.5361 E - 03	5.6980 E - 03	8.0001 E - 03	2.9998 E - 03
7	1.7656 E - 02	1.7103 E - 02	-1.0507 E - 02	1.8545 E - 02
8	3.3677 E - 02	-1.7997 E - 01	-1.6311 E - 01	3.4514 E - 02
9	-3.7643 E - 03	-1.3251 E - 01	1.4597 E - 01	5.3709 E - 02
10	1.7452 E - 02	-6.4239 E - 02	1.0517 E - 01	-1.3732 E - 01
11	-2.1150 E + 02	2.2136 E + 02	3.7357 E + 00	8.6434 E + 01
12	-2.7270 E - 03	2.4859 E - 01	2.4620 E - 01	1.9930 E - 02
13	2.7465 E - 02	-1.7732 E - 01	-5.0845 E - 02	-8.4711 E - 02
14	-9.5216 E + 01	1.0541 E + 02	1.0775 E + 02	8.9339 E + 01
15	-1.3373 E - 01	-1.1071 E + 00	3.9103 E - 01	-4.9083 E - 02
16	-2.7321 E - 02	-3.6255 E - 02	9.6719 E - 02	9.1420 E - 03
17	-9.6732 E - 03	-1.0180 E - 01	1.2624 E - 01	-1.6362 E - 02
18	-1.4584 E + 01	-1.9548 E + 02	-1.6608 E + 01	4.9234 E + 01
19	-2.7469 E - 02	1.1711 E - 01	-1.4463 E - 01	-4.6712 E - 02
20	-1.7398 E + 02	-2.1532 E + 02	1.0964 E + 02	5.2774 E + 01
21	-6.6567 E - 02	-3.1594 E - 01	-2.0686 E - 01	-
22	-5.9604 E - 03	5.2452 E - 02	8.2922 E - 03	-
23	6.7446 E - 03	-3.1686 E - 02	-3.0261 E - 02	-
24	-2.6620 E - 02	-1.3975 E - 01	1.4237 E - 01	-
25	1.4691 E - 02	8.3399 E - 02	-2.8977 E - 02	-
26	-1.0971 E - 01	2.1382 E - 01	2.2409 E - 01	-
27	8.8700 E - 03	-6.1816 E - 02	-7.9313 E - 02	-
28	3.6918 E - 03	-1.5026 E - 02	-1.6385 E - 02	-
29	1.2219 E - 02	1.0574 E - 01	-1.0113 E - 01	-
30	-7.6358 E - 03	-9.7446 E - 02	6.5531 E - 02	-
31	-4.4894 E - 03	2.2606 E - 02	5.3655 E - 02	-
32	2.3646 E - 03	1.2125 E - 02	-2.3722 E - 03	-
33	5.0569 E - 03	-2.2391 E - 02	1.8910 E - 02	-
34	1.0792 E - 03	-2.4648 E - 03	-2.6522 E - 03	-
35	-7.1610 E - 04	3.2432 E - 03	8.3050 E - 03	-
36	9.6385 E - 04	-5.7766 E - 03	-3.8860 E - 03	-

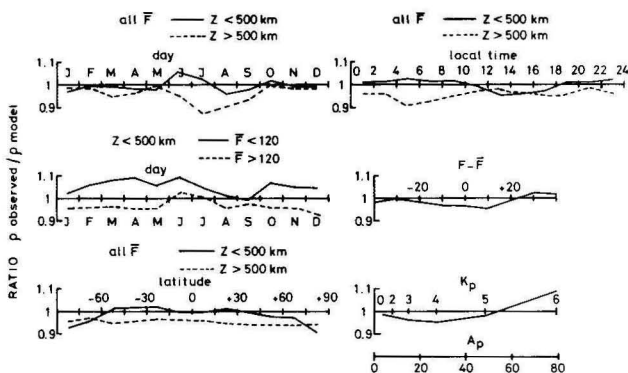


Fig. 2

Ratio between the observed and computed densities as a function of several geophysical parameters.

appears that the departure between the observed and computed densities is less than 10 %, which is rather satisfactory. When the comparison is made only with the 36000 densities used in the spherical harmonic analysis, the mean value of  $\rho_{obs}/\rho_{model}$  is 0.99. When the whole date base is used, the mean value of  $\rho_{obs}/\rho_{model}$  is 0.975. The small difference of 1.5 % results from the fact that some drag data are affected by systematic errors caused by a poor knowledge of the area to mass ratio.

### 3. Some geophysical characteristics of the model

The geophysical variations, which were initially discovered with satellite drag data (see Jacchia, 1972) are of course included in the present model. Using the FORTRAN subroutines given in appendix 1, it is, therefore, possible to analyze the solar activity effect, the geomagnetic effect, the daily variation, the semiannual variation and the seasonal-latitude variation of various geophysical parameters. We present here an overview of some characteristics of our model and leave for a future paper a detailed comparison with existing models.

#### 3.1. Solar activity effect

The solar ultraviolet flux between 175 nm and 10 nm is the major primary energy source which influences the whole terrestrial thermosphere. Measurements are not yet sufficiently numerous to give a quantitative description over a whole eleven year solar cycle. Published data (Hinteregger, 1976; Schmidtke, 1976) refer usually to a specific day with a certain solar activity level. Average values, such as those given by Banks and Kockarts (1973) intend to represent different solar activity levels with a rather poor absolute accuracy. The solar 10.7 cm flux, which has no effect on the thermospheric heating, is therefore used as an index for the solar activity, since it originates in the solar corona where some of the extreme ultraviolet flux (EUV) is produced. Any correla-

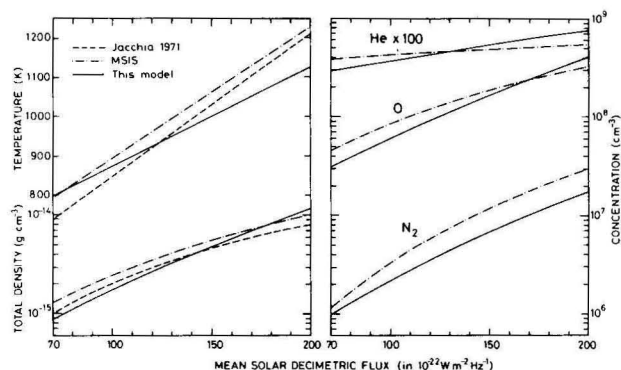


Fig. 3

Temperature, total density and partial concentrations at the equator for an altitude of 400 km as a function of the mean solar decimetric flux  $\bar{F}$ . Comparison with Jacchia 1971 and MSIS models.

tion between the thermopause temperature and the 10.7 cm flux is only a practical way to describe solar activity effects, but it does not necessarily represent correctly the complex physical mechanisms of the interactions between the solar EUV flux and the thermospheric constituents. Figure 3 shows the increase of the thermopause temperature, the total density  $\rho$  and the concentrations  $n(He)$ ,  $n(O)$  and  $n(N_2)$  as a function of the average flux  $\bar{F}$  (with  $F = \bar{F}$ ) over three solar rotations centered on the September equinox (day 264). The computations are made at the geographic equator for an altitude of 400 km and a planetary geomagnetic index  $K_p = 2$ . Since the solar activity effect depends also on the daily flux  $F$  (see eq. 13), the increase of the thermopause temperature,  $\rho$ ,  $n(He)$ ,  $n(O)$  and  $n(N_2)$  is shown on Figure 4 as a function of  $F - \bar{F}$ , with  $\bar{F} = 130$ . The various quantities on Figure 3 and 4 are diurnal averages

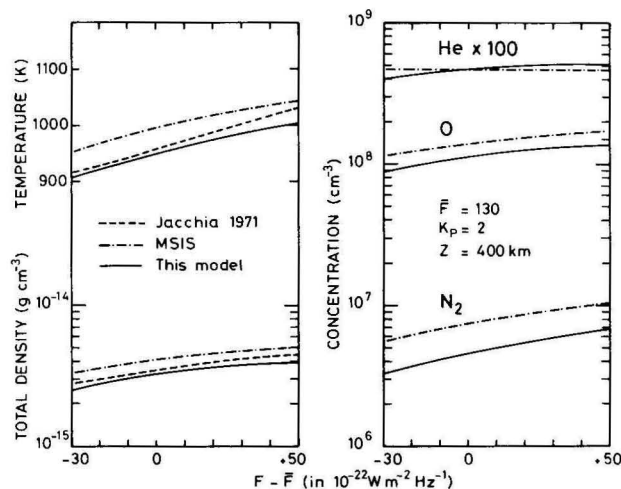


Fig. 4

Temperature, total density and partial concentrations as a function of  $F - \bar{F}$ . Comparison with Jacchia 1971 and MSIS models.

and there is a general increase with solar activity. The results obtained with Jacchia's (1971) model and MSIS (Hedin *et al.*, 1977a, 1977b) are indicated for comparison. The eleven year variation and the 27 days fluctuations should be well represented by the present model based on a large data coverage (see Figure 1).

### 3.2. Geomagnetic activity

The second important energy source is related to the geomagnetic activity represented by the planetary index  $K_p$ . The physical energy input results now from Joule heating and particle precipitations along the geomagnetic field lines (Cole, 1975; Banks, 1977; Dickinson, Ridley and Roble, 1977). As for the 10.7 cm flux, it is clear that  $K_p$  can only be an index which does not necessarily represents the real physical mechanism responsible for the increase of temperature and densities associated with geomagnetic activity.

Considering the way  $K_p$  is introduced in the spherical harmonic expansion (8), it is easily understood that the geomagnetic effect can have a rather strong latitudinal dependence. This is in agreement with the physical heating mechanisms which are more effective in the high latitude regions. Figure 5 gives the variation of the total density and the major constituents as a function of

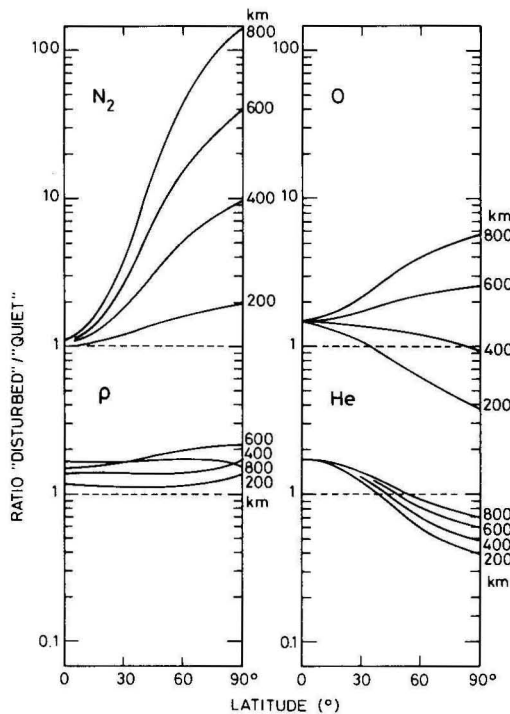


Fig. 5

Latitudinal variation of the geomagnetic effect for  $\rho$ ,  $n(N_2)$ ,  $n(O)$  and  $n(He)$  when  $K_p$  increases from 0 to 5. Computations are made for March equinox with a daily averaged temperature of 900 K (quiet conditions  $K_p = 0$ ) at the equator.

latitude for  $K_p = 5$ . The variations represent the ratio between a model with  $K_p = 5$  and a model with  $K_p = 0$  for which the diurnally averaged thermopause temperature is 900 K at the geographic equator. Results are given for 200 km, 400 km, 600 km and 800 km altitude. At the equator, it appears that the variation is negligible for  $N_2$  whereas an increase of 1.5 is obtained for  $O$  and  $He$ . The variations of the major constituents increases with latitude as a consequence of the temperature behaviour in the model of Thuillier *et al.* (1977b). The geomagnetic effect in this model is responsible for the disappearance of the temperature bulge in the vicinity of the subsolar point. Since the temperature increase with  $K_p$  is more important in the polar region, a large area with high temperature appears at high latitude and smears out the usual temperature bulge.

An increase of  $K_p$  leads always to an increase in  $N_2$  at higher latitude. An increase of  $K_p$  leads, however, to a decrease of  $O$  below 500 km altitude and atomic oxygen has a behavior similar to  $N_2$  only at greater height. For latitudes greater than  $45^\circ$ , helium always decreases with increasing  $K_p$ . The geomagnetic variation of the total density does not depend strongly on the latitude (Jacchia, 1971; Roemer and Lay, 1972), as a consequence of the opposite behavior of  $N_2$ ,  $O$  and  $He$  shown on Figure 5. Latitudinal changes of composition during geomagnetic disturbances have also been analyzed by Jacchia, Slowey and von Zahn (1976) and by Keating, Prior, Chang, Nicholson and von Zahn (1977). These results are similar to those presented on Figure 5.

After a brief presentation of the two major effects (solar and geomagnetic) which result from primary energy inputs, a discussion of some consequential effects will be given in the following subsections.

### 3.3. Daily variation

The general picture of the terrestrial atmosphere will be given for two different solar and geomagnetic activities: high activity ( $F = \bar{F} = 150 \times 10^{-22} \text{ W m}^{-2} \text{ Hz}^{-1}$ ;  $K_p = 2$ ) and low activity ( $F = \bar{F} = 92 \times 10^{-22} \text{ W m}^{-2} \text{ Hz}^{-1}$ ;  $K_p = 1$ ). The high activity corresponds roughly to the average conditions during the operational lifetime of the OGO 6 satellite, whereas the low activity intends to represent the average conditions during the ESRO 4 satellite lifetime.

Figure 6 shows maps for June solstice at an altitude of 400 km for high activity conditions. Low activity conditions for June solstice are represented on Figure 7 for 275 km altitude (mean ESRO IV conditions). Both figures represent the latitudinal dependence of  $\rho$ ,  $n(N_2)$ ,  $n(O)$  and  $n(He)$  as a function of local-time (left part) and day of year (right part). Local time variations will first be discussed.

As in all semi-empirical models, total density goes through a maximum around 14 hours LT. The total den-

sity minimum is, however, broader than in Jacchia's (1971) model and it is located at a rather high latitude on the left parts of Figures 6 and 7 (Barlier *et al.* 1973). The maximum is also spread out and on Figure 6 an absolute maximum of  $\rho$  appears near the equator. Such a fact is explained by the behavior of atomic oxygen (see Figure 5) which is the major component at 400 km altitude. The slow decrease of  $\rho$  towards the north pole is explained by the  $N_2$  maximum and the temperature increase towards the summer pole. Furthermore, the helium bulge (Keating and Prior, 1968) prevents a sharp decrease of the total density towards the winter pole.

The individual constituents have not, however, their maximum at the same local time. With the exception of the absolute maximum near the summer pole (Figure 6) molecular nitrogen peaks around 16-19 hours LT whereas helium has its maximum around 10 hours LT. Atomic oxygen has a maximum around 13-14 hours LT and a small nighttime maximum appears in the equatorial region (Berger, 1976). The time of the daily maximum for each constituent is altitude dependent.

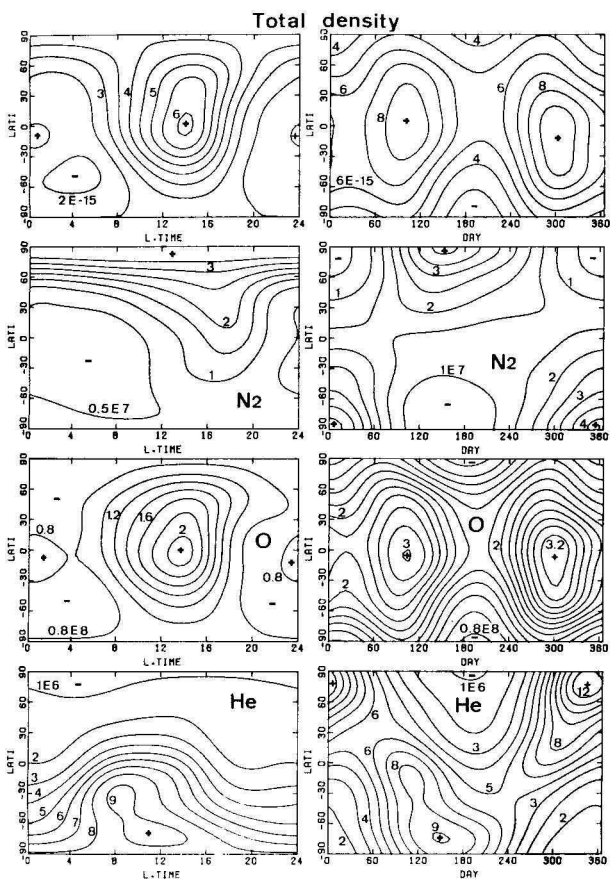


Fig. 6

Diurnal variation of  $\rho$ ,  $n(N_2)$ ,  $n(O)$  and  $n(He)$  at 400 km for June solstice with  $F = \bar{F} = 150 \times 10^{-22} \text{ W m}^{-2} \text{ Hz}^{-1}$  and  $K_p = 2$  (left part). Global annual variation at 15 hours LT for the same quantities (right part).

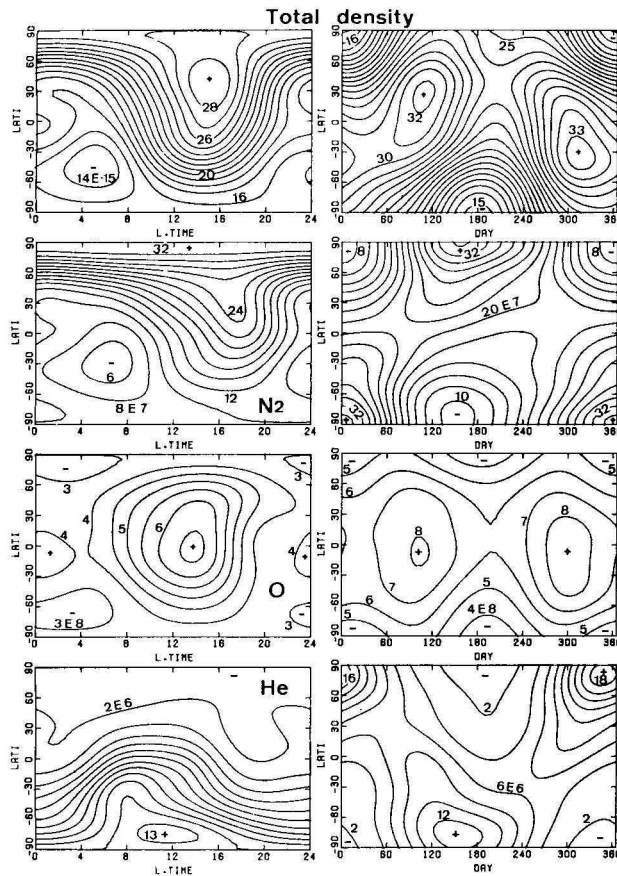


Fig. 7

Diurnal variation of  $\rho$ ,  $n(N_2)$ ,  $n(O)$  and  $n(He)$  at 275 km for June solstice  $F = \bar{F} = 92 \times 10^{-22} \text{ W m}^{-2} \text{ Hz}^{-1}$  and  $K_p = 1$  (left part). Global annual variation at 15 hours LT for the same quantities (right part).

The diurnal variation of  $\rho$ ,  $n(He)$ ,  $n(O)$  and  $n(N_2)$  is given at the equator on Figure 8 for high and low activity conditions at 400 km altitude. The total density of the model of Jacchia (1971) is shown for comparison. Partial concentrations for  $N_2$ ,  $O$  and  $He$  are also reproduced from the MSIS model (Hedin *et al.*, 1977a, 1977b). Although the general behavior is similar, the MSIS model gives values for  $N_2$  which can be at 400 km a factor of two higher than in the present model for  $F = \bar{F} = 150 \times 10^{-22} \text{ W m}^{-2} \text{ Hz}^{-1}$ . This results from the large temperature obtained with MSIS for  $F = \bar{F} = 150 \times 10^{-22} \text{ W m}^{-2} \text{ Hz}^{-1}$  (see Fig. 3).

### 3.4. Annual variations

Figure 9 shows the annual variation of the diurnally averaged total density at 400 km altitude. Computations are made for  $45^\circ\text{N}$  and  $45^\circ\text{S}$  with a constant solar decimetric flux ( $F = \bar{F} = 150 \times 10^{-22} \text{ W m}^{-2} \text{ Hz}^{-1}$ ) and with  $K_p = 2$ . The semiannual variation is clearly indicated with its maximum values around the equinoxes and a

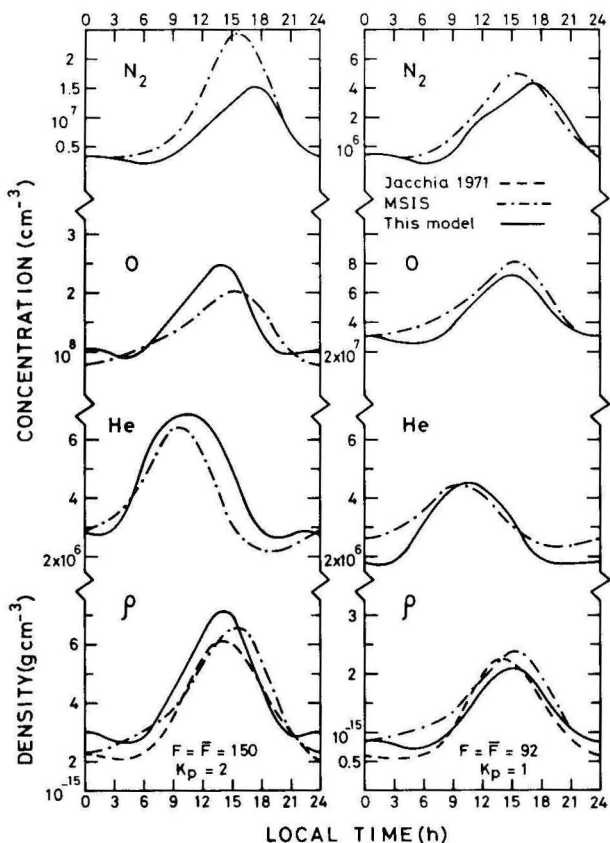


Fig. 8

Diurnal variation of  $\rho$ ,  $n(N_2)$ ,  $n(O)$  and  $n(He)$  at the equator for high and low solar activity at an altitude of 400 km. Comparison with Jacchia 1971 and MSIS models.

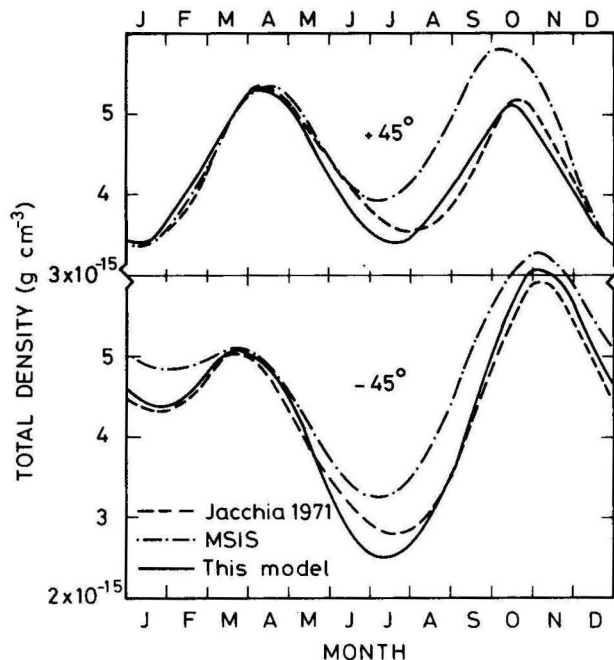
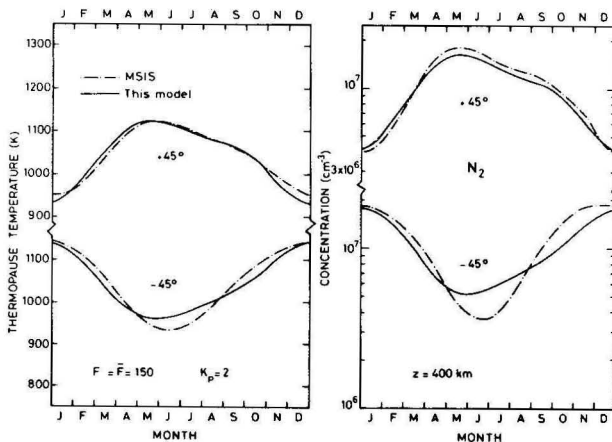


Fig. 9



Annual variation of the thermopause temperature and  $n(N_2)$ . Same condition as in Fig. 9.

Annual variation of  $\rho$  at 400 km altitude for  $45^\circ N$  and  $45^\circ S$  with  $F = \bar{F} = 150 \times 10^{-22} \text{ W m}^{-2} \text{ Hz}^{-1}$  and  $K_p = 2$ . Comparison with Jacchia 1971 and MSIS models.

deep minimum in July. A similar behavior is obtained with Jacchia's model (1971) and with MSIS model (Helin *et al.* 1977b). A strong difference appears, however, between the North and the South. The seasonal effect (difference between local summer and local winter) is in phase with the annual effect in the southern hemisphere and it is in opposite phase in the northern hemisphere. Furthermore, the diurnally averaged density is slightly higher during local spring and this fact is more pronounced in the southern hemisphere. These characteristics are related to the North-South asymmetries discussed by Barrier, Bauer, Jaeck, Thuillier and Kockarts (1974).

Figures 10, 11 and 12 give the annual variations of the major constituents  $N_2$ ,  $O$  and  $He$  for the same conditions as the total density on Figure 9. The thermopause temperature is also shown on Figure 10 since molecular nitrogen has always a similar behavior. For  $N_2$  as well as for the temperature, the maxima around the equinoxes are not very pronounced and the July minimum is very weak in the northern hemisphere. For atomic oxygen (Figure 11) the equinoctial maxima are, however clearly defined. Absolute maxima appear actually near the equator as it is shown in the right hand part of Figures 6 and 7. The annual variation of helium shown on Figure 12 can be compared with the result for  $N_2$  (Fig. 10) if a hemispherical reversal is made. The July minimum is very weak in the southern hemisphere. At 400 km altitude, the behavior of  $N_2$  in the northern hemisphere is similar to the annual variation of  $He$  in the southern hemisphere as a consequence of the winter helium bulge.

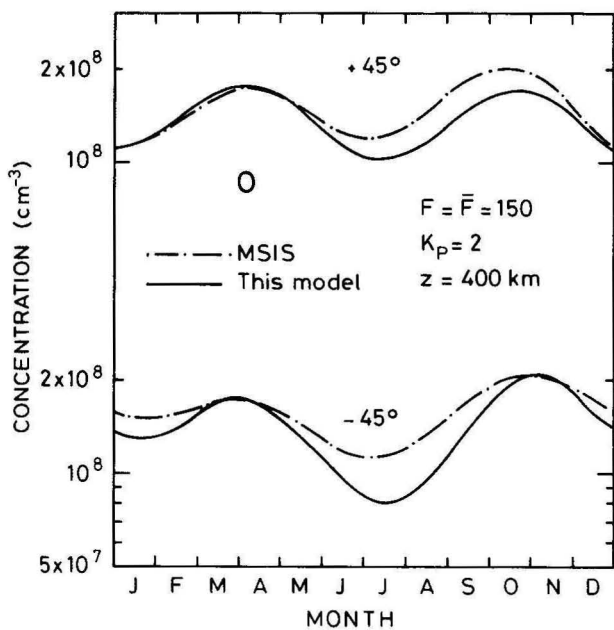


Fig. 11

Annual variation of  $n(O)$ . Same conditions as in Fig. 9.

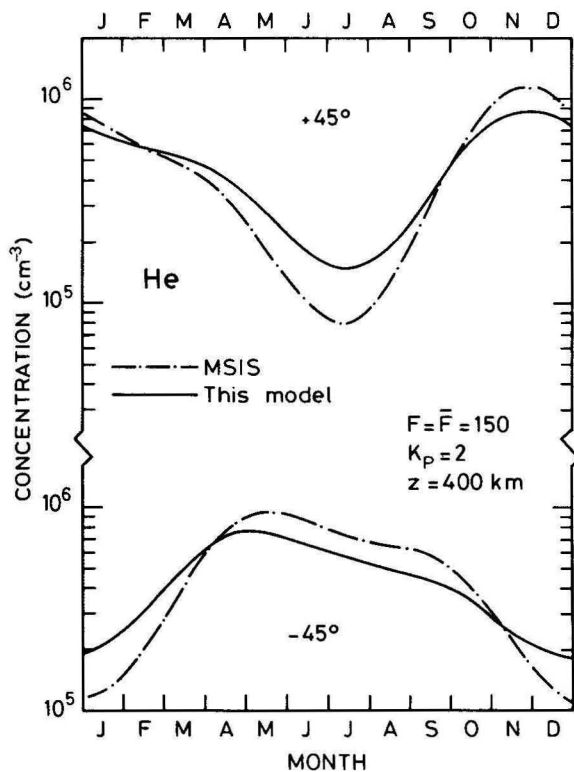


Fig. 12

Annual variation of  $n(He)$ . Same conditions as in Fig. 9.

Information given in Figure 9 to 12 for  $\pm 45^\circ$  latitude can be extended by a discussion of the right hand parts of Figures 6 and 7 which show the global annual variation at 400 km and 275 km for 15 hours LT. The annual variation of  $N_2$  is more pronounced in the polar regions. An absolute maximum for  $N_2$  appears near the northern pole a little before June solstice (day 150). The absolute maxima of  $O$  occur near the equator around 15 April and 30 October, the October maximum being the most important. The winter helium bulge is clearly seen on Figures 6 and 7 and the seasonal variation is larger at the northern pole than at the southern pole, i.e. a behavior in contradiction with the analysis of Keating, McDougal, Prior and Levine (1973).

A comparison of the latitudinal variation of  $He$  with Jacchia's (1971) and the MSIS model (Hedin *et al.* 1977b) is given in Figure 13 for the two solstices. The

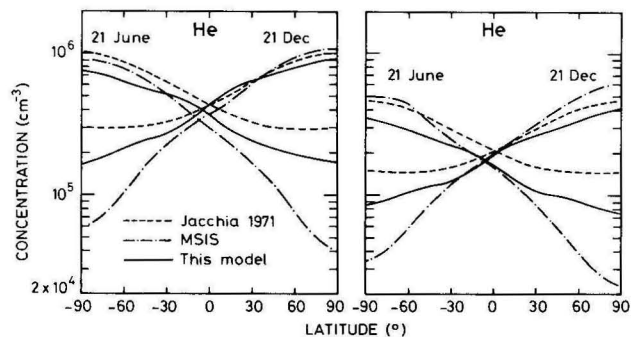


Fig. 13

Latitudinal variation of  $n(He)$  at 1000 km altitude. The left part corresponds to  $F = \bar{F} = 150 \times 10^{-22} \text{ W m}^{-2} \text{ Hz}^{-1}$  and  $K_p = 2$ . The right part corresponds to  $F = \bar{F} = 92 \times 10^{-22} \text{ W m}^{-2} \text{ Hz}^{-1}$  and  $K_p = 2$ . Comparison with Jacchia 1971 and MSIS models.

agreement is rather good for winter conditions when helium reaches its maximum value. During local summer differences larger than a factor of 2 appear between our model and the MSIS model which is based on mass spectrometric determination of helium. It is difficult to reconcile such a large discrepancy with our total density data without questioning the mass spectrometric measurements for low helium abundances (Trinks, von Zahn, Reber, Hedin, Spencer, Krankowsky, Lämmerzahl, Kayser and Nier, 1977).

#### 4. Conclusion

Using 36000 total densities deduced from satellite drag data, a new thermospheric model has been developed in terms of spherical harmonics. Such a model is able to represent the initial data file of 70000 values with an accuracy of the order of 10%. It gives also the

concentrations of helium, atomic oxygen and molecular nitrogen. These quantities have been deduced from the observed total densities by an iterative process. Preliminary comparisons with models based on mass spectrometric measurements justify *a posteriori* the technique used in this paper.

A major advantage of the present model comes from the good temporal and spatial coverage of the initial data which are distributed over almost two solar cycles. Such a time interval is, however, not long enough to ascertain definitively all the physical properties of the terrestrial thermosphere. This is particularly true when one realizes that two solar cycles can be very different from each other. It is, therefore, highly desirable that

the "old" technique of density determination from satellite drag data should be pursued at least during several solar cycles.

#### Acknowledgements

We express our sincere thanks to Dr. L.G. Jacchia who kindly provided us a large amount of satellite drag data. This work has been partially supported through RCP 336 and by the French CNRS, DRME and CNES.

Manuscrit reçu le 10-10-77

#### APPENDIX 1

SUBROUTINE MODEL (DAY, F, FBAR, AKP, ALTI, HL, ALAT, TZ, TINF, DHELIO, DOXY,  
\* DN2, DO2, DTOTAL)

CC

```
C INPUT
C DAY = DAY NUMBER IN THE YEAR
C F = 10.7 FLUX FOR DAY-1
C FBAR = MEAN FLUX
C AKP = KP INDEX 3 HOURS BEFORE HL
C ALTI = ALTITUDE IN KM
C HL = LOCAL TIME
C ALAT = LATITUDE IN DEGREES
C OUTPUT
C TZ = TEMPERATURE AT ALTITUDE ALTI
C TINF = THERMOPAUSE TEMPERATURE
C DHELIO = HELIUM CONCENTRATION (CM-3) AT HEIGHT ALTI
C DOXY = ATOMIC OXYGEN CONCENTRATION (CM-3)
C DN2 = MOLECULAR NITROGEN CONCENTRATION (CM-3)
C DO2 = MOLECULAR OXYGEN CONCENTRATION (CM-3)
C DTOTAL = TOTAL DENSITY (G/CM3)
```

CC

```
C
C DIMENSION A(36), B(36), C(36), OGO(36), ALEFA (5), MA(5), D(5), DBASE(5)
C COMMON /POL/P10, P20, P30, P40, P50, P11, P21, P31, P51, P22, P32, P33
C TEMPERATURE
C DATA OGO/999.8,
C * -0.36357E-02, 0.24593E-01, 0.13259E-02, -0.56234E-05, 0.25361E-02,
C * 0.17656E-01, 0.33677E-01, -0.37643E-02, 0.17452E-01, -0.21150E 03,
C * -0.27270E-02, 0.27465E-01, -0.95216E 02, -0.13373E 00, -0.27321E-01,
C * -0.96732E-02, -0.14584E 02, -0.27469E-01, -0.17398E 03, -0.66567E-01,
C * -0.59604E-02, 0.67446E-02, -0.26620E-01, 0.14691E-01, -0.10971E 00,
C * 0.88700E-02, 0.36918E-02, 0.12219E-01, -0.76358E-02, -0.44894E-02,
C * 0.23646E-02, 0.50569E-02, 0.10792E-02, -0.71610E-03, 0.96385E-03/
```

```

C   HELIUM
    DATA A/3.E 07,
*   0.16926E 00, -0.62624E-01, 0.23799E-02, -0.31008E-04, 0.56980E-02,
*   0.17103E-01, -0.17997E 00, -0.13251E 00, -0.64239E-01, 0.22136E 03,
*   0.24859E 00, -0.17732E 00, 0.10541E 03, -0.11071E 01, -0.36255E-01,
*   -0.10180E 00, -0.19548E 03, 0.11711E 00, -0.21532E 03, -0.31594E 00,
*   0.52452E-01, -0.31686E-01, -0.13975E 00, 0.83399E-01, 0.21382E 00,
*   -0.61816E-01, -0.15026E-01, 0.10574E 00, -0.97446E-01, 0.22606E-01,
*   0.12125E-01, -0.22391E-01, -0.24648E-02, 0.32432E-02, -0.57766E-02/

C   ATOMIC OXYGEN
    DATA B/1.032E 11,
*   -0.16598E-02, -0.99095E-01, 0.78453E-03, -0.23733E-04, 0.80001E-02,
*   -0.10507E-01, -0.16311E 00, 0.14597E 00, 0.10517E 00, 0.37357E 01,
*   0.24620E 00, -0.50845E-01, 0.10775E 03, 0.39103E 00, 0.96719E-01,
*   0.12624E 00, -0.16608E 02, -0.14463E 00, 0.10964E 03, -0.20686E 00,
*   0.82922E-02, -0.30261E-01, 0.14237E 00, -0.28977E-01, 0.22409E 00,
*   -0.79313E-01, -0.16385E-01, -0.10113E 00, 0.65531E-01, 0.53655E-01,
*   -0.23722E-02, 0.18910E-01, -0.26522E-02, 0.83050E-02, -0.38860E-02/

C   MOLECULAR NITROGEN
    DATA C/3.842E 11,
*   0.28076E-01, 0.48462E-01, -0.81017E-03, 0.20983E-04, 0.29998E-02,
*   0.18545E-01, 0.34514E-01, 0.53709E-01, -0.13732E 00, 0.86434E 02,
*   0.19930E-01, -0.84711E-01, 0.89339E 02, -0.49083E-01, 0.91420E-02,
*   -0.16362E-01, 0.49234E 02, -0.46712E-01, 0.52774E 02, 0.          ,
*   0.          , 0.          , 0.          , 0.          , 0.          ,
*   0.          , 0.          , 0.          , 0.          , 0.          ,
*   0.          , 0.          , 0.          , 0.          , 0.          /

    DATA T02/4.775E + 10/
    DATA ALEFA/0., -0.38, 0., 0., 0./
    DATA MA/1,4, 16, 28, 32/
    DATA RE/6356.77/, GSURF/980.665/, RGAS/8.314 + 2/, ZLB/120./, S/0.02/
    CALL POLYNO(ALAT)
    GALL GDELRB(ALAT, FBAR, F, AKP, DAY, HL, OGO, GDELT, 1.)
    TINF = OGO(1)*GDELT
    CALL GDELRB(ALAT, FBAR, F, AKP, DAY, HL, A, GDELH, 0.)
    DBASE(2) = A(1)*EXP(GDELH-1.)
    CALL GDELRB(ALAT, FBAR, F, AKP, DAY, HL, B, GDELO, 1.)
    DBASE(3) = B(1)*EXP(GDELO-1.)
    CALL GDELRB(ALAT, FBAR, F, AKP, DAY, HL, C, GDELN, 1.)
    DBASE(4) = C(1)*EXP(DGELN-1.)
    DBASE(5) = TO2
    SIGMA = S + 1./(RE + ZLB)
    ZETA = (ALTI-ZLB)*(RE + ZLB)/(RE + ALTI)
    EXPSZ = EXP(-SIGMA*ZETA)
    TZ = TINF-(TINF-380.)*EXPSZ
    GLB = GSURF/(1. + ZLB/RE)**2
    AA = 1.-380./TINF
    DO 1 I = 2, 5
    GAMMA = MA(I)*GLB/(SIGMA*RGAS*TINF)
    D(I) = DBASE(I)*((1.-AA)/(1.-AA*EXPSZ))**(1. + ALEFA(I) + GAMMA)
    *EXP(-SIGMA*GAMMA*ZETA)
    1 CONTINUE
    DHELIO = D(2)
    DOXY = D(3)

```

```

DN2 = D(4)
DO2 = D(5)
DTOTAL = 1.6603E-24* (4.*D(2) + 16.*D(3) + 28.*D(4) + 32.*D(5))
RETURN
END
SUBROUTINE GDELRB(ALAT, FBAR, F, AKP, DAY, HL, A, GDEL, FFO)

```

```

C COMPUTATION OF G(L)
C A = VECTOR OF COEFFICIENTS FOR G(L)
C FFO = 1 FOR ATOMIC OXYGEN, NITROGEN AND TEMPERATURE
C FFO = 0 FOR HELIUM
C GDEL = VALUE OF G(L)
C
DIMENSION A(36)
COMMON /POL/P10, P20, P30, P40, P50, P11, P21, P31, P51, P22, P32, P33
DATA PI/3.141592/
ROT1 = 2.*PI/24.
ROT2 = 2.*PI/365.
COSTE = COS(ROT2*(DAY-A(18)))
DELTF = F - FBAR
FO = A(4)*DELTF + A(5)*DELTF**2 + A(6)*(FBAR-150.)
F1F = 1. + FO*FFO
G7 = 1.
DCH = A(29)*P11 + A(30)*P21
CCH = A(24)*P11 + A(25)*P21
ACH = A(21)*P11 + A(22)*P31 + A(23)*P51
BCH = A(26)*P11 + A(27)*P31 + A(28)*P51
G8 = G7 + (ACH + CCH*COSTE)*F1F*COS(HL*ROT1)
G9 = G8 + (BCH + DCH*COSTE)*F1F*SIN(HL*ROT1)
G10 = G9 + (A(31)*P22 + A(32)*P32*COSTE)*F1F*COS(HL*ROT1*2.)
G11 = G10 + (A(33)*P22 + A(34)*P32*COSTE)*F1F*SIN(HL*ROT1*2.)
G12 = G11 + A(35)*P33*F1F*COS(3.*HL*ROT1)
G13 = G12 + A(36)*P33*F1F*SIN(3.*HL*ROT1)
X2 = G13 + FO + A(2)*P20 + A(3)*P40
X3 = X2 + (A(7) + A(8)*P20)*AKP
X4 = X3 + (A(9) + A(10)*P20)*COS(ROT2*(DAY-A(11)))*F1F
X5 = X4 + (A(12) + A(13)*P20)*COS(2.*ROT2*(DAY-A(14)))*F1F
X6 = X5 + (A(15)*P10 + A(16)*P30 + A(17)*P50)*F1F*COSTE
X7 = X6 + A(19)*P10*COS(2.*ROT2*(DAY-A(20)))*F1F
GDEL = X7
RETURN
END

```

```

SUBROUTINE POLYNO (ALAT)

```

```

C LEGENDRE : ASSOCIATED FUNCTIONS
COMMON /POL/P10, P20, P30, P40, P50, P11, P21, P31, P51, P22, P32, P33
DATA PI/3.141592/
COLAT = 90.-ALAT
CALAT = COLAT*PI/180.
R = COS(CALAT)
R2 = R**2
R4 = R2**2
RR = SIN(CALAT)
P10 = R
P20 = 0.5*(3.*R2-1.)

```

```

P30 = 0.5*R*(5.*R2-3.)
P40 = 0.125*(35.*R4-30.*R2 + 3.)
P50 = 0.125*R*(63.*R4-70.*R2 + 15.)
P11 = RR
P21 = RR*3.*R
P31 = RR*1.5*(5.*R2-1.)
P51 = (RR*15.*(21.*R4-14.*R2 + 1.))/8.
P22 = 3.*(RR**2)
P32 = 15.*R*(RR**2)
P33 = 15.*(RR**3)
RETURN
END

```

## References

- Alcaydé D., Bauer P. and Fontanari J., "Long-term variations of thermospheric temperature and composition", *J. Geophys. Res.*, **79**, 629-637, 1974.
- Alcaydé D., Bauer P., Hedin A.E. and Salah J.E., "Compatibility of seasonal variations in midlatitude thermospheric models at solar maximum and low geomagnetic activity", *J. Geophys. Res.*, **82**, to be published, 1977.
- Banks P.M., "Observations of Joule and particle heating in the auroral zone", *J. Atmos. Terr. Phys.*, **39**, 179-193, 1977.
- Banks P.M. and Kockarts G., "Aeronomy, Part A, p. 49, p. 163, Academic Press, New York, 1973.
- Barlier F., Bauer P., Jaeck C., Thuillier G. and Kockarts G., "North-South asymmetries in the thermosphere during the last minimum of the solar cycle", *J. Geophys. Res.*, **79**, 5273-5285, 1974.
- Barlier F., Falin J.L., III M. and Jaeck C., "Structure of the neutral atmosphere between 150 and 500 km", *Space Research*, **13**, 349-355, 1973.
- Bates D.R., "Some problems concerning the terrestrial atmosphere above about the 100 km level", *Proc. Roy. Soc.*, **A253**, 451-462, 1959.
- Berger C., "Analyse et modélisation statistique de différents paramètres de l'atmosphère neutre - Asymétries hémisphériques". Thèse de doctorat d'Etat, Université Pierre et Marie Curie, Paris, 1976.
- Cole K.D., "Energy deposition in the thermosphere caused by the solar wind", *J. Atmos. Terr. Phys.*, **37**, 939-949, 1975.
- Cook G.E., "Drag coefficients of spherical satellites", *Ann. Géophys.*, **22**, 53-64, 1966.
- Dickinson R.E., Ridley E.C. and Roble R.G., "Meridional circulation in the thermosphere. II. Solstice conditions", *J. Atmos. Sci.*, **34**, 178-192, 1977.
- Donahue T.M. and Carignan G.R., "The temperature gradient between 100 and 120 km", *J. Geophys. Res.*, **80**, 4565-4569, 1975.
- Fernandez Salgado, "Etude comparative des variations de densité totale à l'aide de l'analyse factorielle de correspondance", Thèse de 3<sup>ème</sup> cycle, Université de Paris VI, 1976.
- Groves G.V., "Air density in the upper atmosphere from satellite orbit observations", *Nature*, **184**, 178-179, 1959.
- Hedin A.E., Mayr H.G., Reber C.A., Spencer N.W. and Carignan G.R., "Empirical model of global thermospheric temperature and composition based on data from the OGO 6 quadrupole mass spectrometer", *J. Geophys. Res.*, **79**, 215-225, 1974.
- Hedin A.E., Salah J.E., Evans J.V., Reber C.A., Newton G.P., Spencer N.W., Kayser D.C., Alcaydé D., Bauer P., Cogger L. and McClure J.P., "A global thermospheric model based on mass spectrometer and incoherent scatter data. MSIS 1.  $N_2$  density and temperature", *J. Geophys. Res.*, **82**, 2139-2147, 1977a.
- Hedin A.E., Reber C.A., Newton G.P., Spencer N.W., Brinton H.C. and Mayr H.G., "A global thermospheric model based on mass spectrometer and incoherent scatter data. MSIS 2. Composition", *J. Geophys. Res.*, **82**, 2148-2156, 1977b.
- Hinteregger H.E., "EUV fluxes in the solar spectrum below 2000 Å", *J. Atmos. Terr. Phys.*, **38**, 791-806, 1976.
- Jacchia L.G., "Two atmospheric effects in the orbital acceleration of artificial satellites", *Nature*, **183**, 526-527, 1959.
- Jacchia L.G., "Static diffusion models of the upper atmosphere with empirical temperature profiles", *Smith. Contrib. Astrophys.*, **8**, 215-257, 1965.
- Jacchia L.G., "Revised static models of the thermosphere and exosphere with empirical temperature profiles", *Smith. Astrophys. Obs. Spec. Rep.*, **332**, 113 pp., 1971a.
- Jacchia L.G., private communication 1971b.
- Jacchia L.G., "Atmospheric models in the region from 110 to 2000 km", pp. 277-338, CIRA 1972, Akademie-Verlag, Berlin, 1972.
- Jacchia L.G. and Slowey J.W., "Accurate drag determinations for eight artificial satellites; atmospheric densities and temperatures", *Smith. Astrophys. Obs. Spec. Rep.*, **100**, 177 pp., 1962.
- Jacchia L.G. and Slowey J.W., "A catalog of atmospheric densities from the drag on five balloon satellites", *Smith. Astrophys. Obs. Spec. Rep.*, **368**, 423 pp., 1975.
- Jacchia L.G., Slowey J.W. and von Zahn U., "Latitudinal changes of composition in the disturbed thermosphere from ESRO 4 measurements", *J. Geophys. Res.*, **81**, 36-42, 1976.

- Keating G.M., McDougal D.S., Prior E.J. and Levine J.S., "North-south asymmetry of the neutral exosphere, *Space Research*, 13, 327-335, 1973.
- Keating G.M. and Prior E.J., "The winter helium bulge", *Space Research*, 8, 982-992, 1968.
- Keating G.M., Prior E.J., Chang K., Nicholson J.Y. III and von Zahn U., "Comparison of drag and mass spectrometer measurements during small geomagnetic disturbances", *Space Research*, 17, 355-361, 1977.
- King-Hele D.G., "Methods of determining air density from satellite orbits", *Ann. Géophys.*, 22, 40-52, 1966.
- King-Hele D.G. and Walker D.M.C., "Irregularities in the density of the upper atmosphere : results from satellites", *Nature*, 527-529, 1959.
- Kockarts G., "L'effet de la diffusion thermique sur la distribution de l'hélium dans l'hétérosphère", *Bull. Acad. Roy. Belgique, Classe des Sciences*, 49, 1136-1147, 1963.
- Kockarts G., Neutral atmosphere modeling, pp. 235-243 in B.M. McCormac (ed.) *Atmospheres of Earth and the Planets*, D. Reidel, Dordrecht-Holland, 1975.
- Kockarts G. et Nicolet M., "L'hélium et l'hydrogène atomique au cours d'un minimum d'activité solaire", *Ann. Géophys.*, 19, 370-385, 1963.
- Priester W., "Sonnenaktivität und Abbremsung der Erdsatelliten", *Naturwiss, Dtsch.* 46, 197-198, 1959.
- Roemer M., Die Dichte der Hochatmosphäre und ihre Variationen während der Phase abklingender Sonnenaktivität 1958-1962, Veröffentlichungen der Universitäts-Sternwarte zu Bonn, 1963.
- Roemer M. and Lay G., "Characteristics of the geomagnetic activity effect in the thermosphere", *Space Research*, 12, 797-802, 1972.
- Schmidtke G., "EUV indices for solar-terrestrial relations", *Geophys. Res. Letters*, 3, 573-576, 1976.
- Thuillier G., Falin J.L. and Wachtel C., "Experimental global model of the exospheric temperature based on measurements from the Fabry-Perot interferometer on board the OGO-6 satellite", *J. Atmos. Terr. Phys.*, 39, 399-414, 1977a.
- Thuillier G., Falin J.L. and Barlier F., "Global exospheric model of the exospheric temperature using optical and incoherent scatter measurements", *J. Atmos. Terr. Phys.*, 39, to be published, 1977b.
- Trinks H., von Zahn U., Reber C.A., Hedin A.E., Spencer N.W., Krankowsky D., Lämmerzahl P., Kayser D.C. and Nier A.O., "Intercomparison of neutral composition measurements from the satellites ESRO 4, AEROS A, AEROS B and Atmosphere Explorer C", *J. Geophys. Res.*, 82, 1261-1265, 1977.
- Vercheval J., "Contribution à l'étude de l'atmosphère terrestre supérieure à partir de l'analyse orbitale des satellites", *Acad. Roy. Bel. Mém. Cl. Sci.*, 41, fasc. 6, 183, pp., 1974.
- von Zahn U., Köhnlein W., Fricke K.H., Laux U., Trinks H. and Volland H., "ESRO 4 model of global thermospheric composition and temperatures during times of low solar activity", *Geophys. Res. Letters*, 4, 33-36, 1977.
- Walker J.C.G., "Analytic representation of upper atmosphere densities based on Jacchia's static diffusion models", *J. Atmos. Sci.*, 22, 462-463, 1965.
- Zimmerman S.P. and Keneshea T.J., "The thermosphere in motion", *J. Geophys. Res.*, 81, 3187-3197, 1976.